ChemElectroChem

Research Article
doi.org/10.1002/celc.202400109

Chemistry Europe
European Chemical Societies Publishing

www.chemelectrochem.org

How Metal/Insulator Interfaces Enable an Enhancement of the Hydrogen Evolution Reaction Kinetics

Thomas L. Maier,[a] Lucas B. T. de Kam,[a] Matthias Golibrzuch,[b] Tina Angerer,[a] Markus Becherer,[b] and Katharina Krischer*[a]

The nanostructuring of electrodes is a common way of increasing electrocatalytic activity. Yet, the fact that the presence of insulating material in nanostructured composites can have a positive effect on efficiency was an unexpected recent finding. The rate enhancement has been linked to different electric fields at the insulator and metal interfaces, facilitating enhanced transport of reaction products into the bulk electrolyte. In this article, we further uncover the origin of the rate enhancement with parameter studies and simulations. We experimentally investigate various parameter dependencies of the alkaline Hydrogen Evolution Reaction (HER) on well-defined nanometer-sized Au arrays embedded in a silicon nitride insulating layer. We find a significant enhancement of the HER for all experimental conditions and opposite activity trends with pH, electrolyte concentration and the cationic species compared to a continuous Au electrode. Using a mean field model, we quantify the electrostatic interfacial pressure above the Au and the insulator patches. Combining the double layer simulations with rate equations, we demonstrate that all parameter variations can be consistently explained by the fact that the double layer structure above the insulator patches is much less rigid than above the metal islands and is independent of the applied potential.

Introduction

The use of composite, non-homogeneous, or nanostructured surfaces as catalysts is a promising approach in applied electrocatalysis, as they often show a strongly altered electrocatalytic behavior compared to homogeneous surfaces.[1–4] The improved activity is often ascribed to synergistic effects that lead to more favorable energetics of adsorbed reaction intermediates,[5,6] allow for bifunctional catalysis,[1,2] or cause changes in the structure of the double layer or to non-covalent interactions between hydrated cations in the OHP and adsorbed OH.[3,7–10] A model system for fundamental studies of such composite electrodes is the alkaline Hydrogen Evolution Reaction (HER), which is also of enormous importance for water electrolysis, and which we further consider here.

The HER is a two-electron transfer reaction consisting of electrochemical (Volmer, Heyrovsky) or chemical (Tafel) elementary steps. In alkaline media, these steps are given by Eqs. (1–3), respectively:

$$\text{Volmer}: \quad H_2O + e^- + * \rightarrow H_{ad} + OH^- \tag{1}$$

$$\text{Heyrovsky}: \quad H_2O + H_{ad} + e^- \rightarrow H_2 + OH^- + * \tag{2}$$

$$\text{Tafel}: \quad 2H_{ad} \rightarrow H_2 + 2* \tag{3}$$

Here * denotes a free adsorption site. There are multiple examples in the literature showing that HER kinetics can be altered significantly on laterally structured interfaces[3,4,11–3] compared to bare metal surfaces. Danilovic et al.[2] showed that the coverage of various metal surfaces by metal-oxide particles (in particular $Ni(OH)_2$ nanoparticles) can enhance the HER kinetics significantly. The authors explained the enhancement by a bifunctional role of the metal/particle interface, which promotes the water dissociation. McCrum et al.[14] further elucidated the role of the supporting (transition-)metal for the hydroxide binding strength. They reported a volcano shaped curve for the HER activity as a function of the hydroxide adsorption energy, which makes the OH_{ad} binding energy of the support an additional descriptor. Ledezma-Yanez et al.[8] proposed another explanation for the observed enhancement of $Ni(OH)_2$ decorated metal surfaces: They demonstrated that the introduction of the metal-oxide changes the point-of-zero-charge of the surface, which, in turn, alters the double layer rigidity, thereby lowering the energy barrier necessary for the reorganization of the interfacial water layer and, thus, facilitates the transport of hydroxide ions into the electrolyte bulk. Despite these various studies and attempts to explain the enhancement of alkaline HER rate by metal-oxide particles on metal catalysts, the mechanism is still debated in the literature.[1,2,8,15,16]

Recently, we have demonstrated another way to increase electrochemical reaction rates, namely by using nanostructured

[a] Dr. T. L. Maier, L. B. T. de Kam, T. Angerer, Prof. Dr. K. Krischer
Nonequilibrium Chemical Physics, Department of Physics,
Technical University of Munich,
85748 Garching, Germany
E-mail: krischer@tum.de

[b] Dr. M. Golibrzuch, Prof. Dr. M. Becherer
Nano and Quantum Sensors, Department of Electrical and Computer Engineering, Technical University of Munich,
85748 Garching, Germany

Supporting information for this article is available on the WWW under https://doi.org/10.1002/celc.202400109

electrodes consisting of electroactive metal islands surrounded by insulating material.[3] In particular, we have shown that the HER rate on electrodes consisting of a well-defined array of Au structures embedded in a silicon oxide insulator layer is strongly enhanced compared to the corresponding non-structured bare metal surfaces.

In this manuscript we further explore the properties of such nanostructured electrodes, whereby the silicon oxide insulating layer is replaced by a silicon nitride insulating layer because of its much better stability in alkaline solutions. By varying several properties of the electrolyte, in particular the cationic species, cation concentration, and the pH, we uncover the unique role of metal/insulator interfaces and elaborate a novel reaction mechanism of alkaline HER. In addition, we use advanced double layer models and the concept of electrostatic pressure, which can be considered a measure of the rigidity of the double layer, to derive a qualitative model for the HER current density on metal/insulator interfaces. The results of the simulations capture all experimentally observed trends and, thus, support the proposed mechanism. Overall, we illustrate how electrodes consisting of lateral metal/insulator interfaces allow to tune the properties of the double layer as well as to exploit the different chemical micro-environments on the different materials.

Results and Discussion

HER Activity Dependence on Electrolyte Properties

In the following, we compare the activity of HER from water reduction of a bare polycrystalline gold surface (continuous) with a nanostructured gold surface (nanostructured). The nanostructured electrodes consist of a silicon-based substrate, whose surface is covered by arrays of metal nano-islands embedded in an insulator (silicon nitride) layer. This results in a laterally structured surface that is exposed to the electrolyte. The diameter of the circular nanostructures is 75 nm, their center-to-center distance 150 nm. A schematic intersection of the nanostructured electrode is shown in Figure 1(a) and an exemplary SEM image depicting the top view of an array of nanostructures in Figure 1(b). Exemplary CVs of the two electrode types can be found in SI.1.

The nanostructuring creates a large metal/insulator interfacial length, which can yield strongly altered rates of electrocatalytic reactions. In a previous paper we reported that the gold/silicon oxide interface exhibits a drastically increased HER rate compared to a bare gold surface.[3] The strongly enhanced rate occurs also at gold/silicon nitride interfaces, cf. SI.2, which we use here due to the superior stability of silicon nitride in alkaline solution. Note that silicon nitride is also terminated by OH groups when in contact with an aqueous electrolyte.[17] In addition, this enhancement is not only limited to Au-based catalysts, but is also present for Cu and Pt based catalysts, cf. SI.3. In this section we discuss how the increased rate depends on several electrolyte properties. From these results we elaborate an altered HER mechanism, which occurs at the metal/insulator interface.

Dependence on the Cationic Species

First, we compare the alkaline HER rate of the continuous and nanostructured Au electrodes when the cationic species present in the electrolyte are changed. Figure 2(a) shows linear scan voltammograms (LSVs) of the two systems in alkaline medium with various alkali metal cation species in solution (0.1 M *AM*OH with *AM* = Li, Na, K, Cs; pH 13 for all electrolytes).

The HER activity of the continuous Au layer electrode (Figure 2(a) top) depends significantly on the nature of the cation species and increases in the following order: Li < Na < K < Cs. Thus, the activity increases systematically down the periodic table, i.e. with decreasing degree of solvation of the ions. This behavior is known from Refs. [6, 9, 10] and traced back to a differing net cation concentration at the electrode surface, which originates form different sizes of the solvated cations.[9]

The trend of the nanostructured electrode (Figure 2(a) bottom) behaves completely differently: First, we note that it exhibits a higher HER activity compared to the continuous layer in all four electrolytes. This higher activity is of kinetic origin, cf. SI.4. In addition, the „activity order" is changed, it is ranked from lowest to highest: Cs < Na ≈ Li < K. A similar trend can also be found in neutral electrolyte, cf. SI.5.

Let us analyze the HER activities more quantitatively. Figure 2(b) shows the Tafel analysis of the considered data. The upper panel displays the Tafel slopes for two electrode types

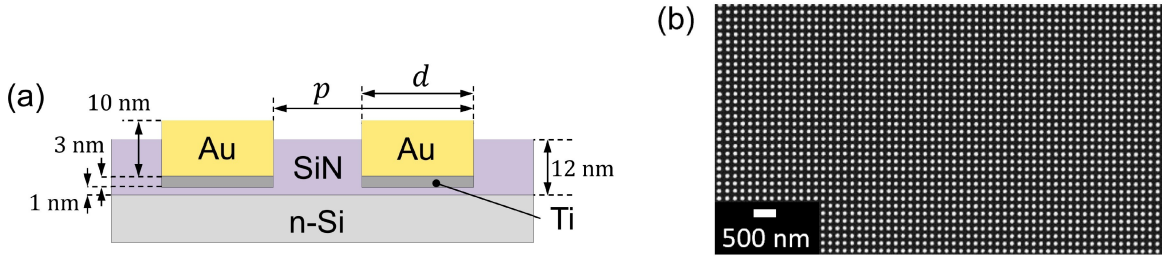

Figure 1. (a) Schematic cross section of the investigated nanostructured electrodes. The size of individual circular structures is $d = 75$ nm. The pitch of the nanostructure array (center distance) is $p = 150$ nm. (b) Exemplary SEM image of a nanostructure array. White: Gold structures, Dark: silicon nitride surface surrounding the gold structures.

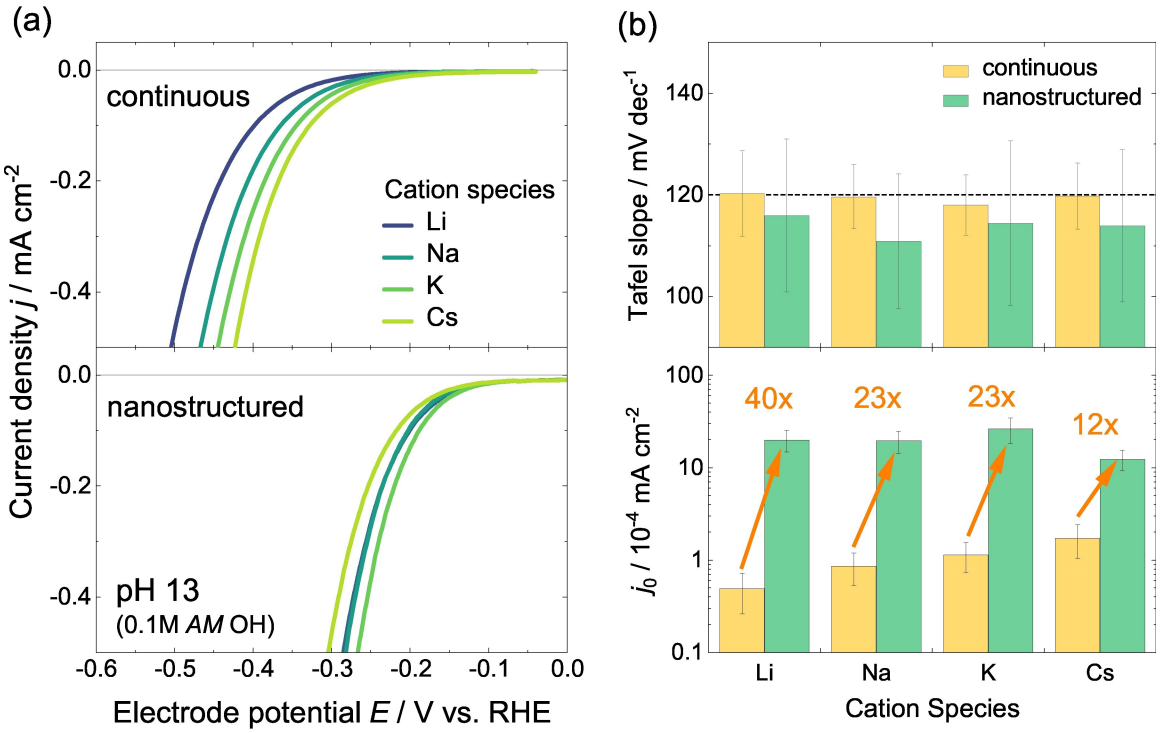

Figure 2. Dependence of the HER activity on the cationic species. (a) LSVs in 0.1 M *AM*OH electrolyte (pH 13) for different alkali metal cations (*AM* = Li, Na, K, Cs) and electrode systems: A continuous gold layer (top), and a nanostructured electrode with a large metal/insulator interface (bottom). (b) Tafel slopes (top) and exchange current densities j_0 (bottom) of the two electrode systems for various cationic species. For all cationic species the Tafel slopes are rather similar, while the exchange current density is significantly larger for the nanostructured electrode.

and the various cationic species, the lower panel depicts the corresponding exchange current densities j_0. We can make the following observations: (1) The Tafel slopes of all the different electrode/cation combinations are rather similar with values around 120 mV dec^{-1} (cf. dashed line in the figure). This slope is well in accordance with results found in the literature for gold-based electrodes in alkaline media.[9,10] This suggests that on continuous and nanostructured Au electrodes and for all cationic species considered here, the HER rate is determined by the first electron transfer step, i.e. the Volmer step. (2) The comparison of the determined exchange current densities (Figure 2(b) bottom) shows that there is a huge difference of HER kinetics between the continuous Au layer and the nanostructured electrode.

Figure 2(a) reveals a complicated dependence of the HER on the type of electrode (nanostructured or continuous electrode) and the nature of the cation. This can be disentangled by comparing the HER activity on the continuous and the nanostructured electrodes individually for each cation. Therefore, we introduce a „cationic enhancement factor" F_{AM}, which is defined as the ratio between j_0 of the nanostructured electrode and j_0 of the continuous layer for a specific cationic species *AM*, cf. Eq. (4):

$$F_{AM} = \frac{j_{0,AM}\,(\text{nanostructured})}{j_{0,AM}\,(\text{continuous})} \tag{4}$$

F_{AM} thus yields directly the enhancement of the HER rate on the nanostructured surface compared to the continuous electrode for the given cationic species. From the data (Figure 2(b) bottom) we derive the following enhancement factors: $F_{Li} \approx 40$, $F_{Na} \approx 23$, $F_K \approx 23$, and $F_{Cs} \approx 12$ (see orange arrows in the figure) which follow a systematic trend:

$$F_{Cs} < F_K \approx F_{Na} < F_{Li} \tag{5}$$

Thus, F_{AM} increases with increasing degree of solvation. Consequently, the HER activity at the metal/insulator interface shows the opposite trend with the cationic species as the continuous Au layer.

In the later section „HER current on nanostructured interfaces", we discuss a model that reproduces this reverse cation trend and suggests that its origin is due to a combination of the acidic nature of the SiOH groups and the different electrostatic pressures across the metal and insulator surfaces.

Dependence on the Electrolyte pH

Next, we consider the activity of the two electrode types when varying the electrolyte pH. Figure 3(a) shows LSVs obtained in an alkaline electrolyte (pH 13, 0.1 M KOH) and in a buffered neutral electrolyte (pH 7, 0.18 M KOH + 0.12 M $H_2PO_4^-$/HPO_4^{2-}).

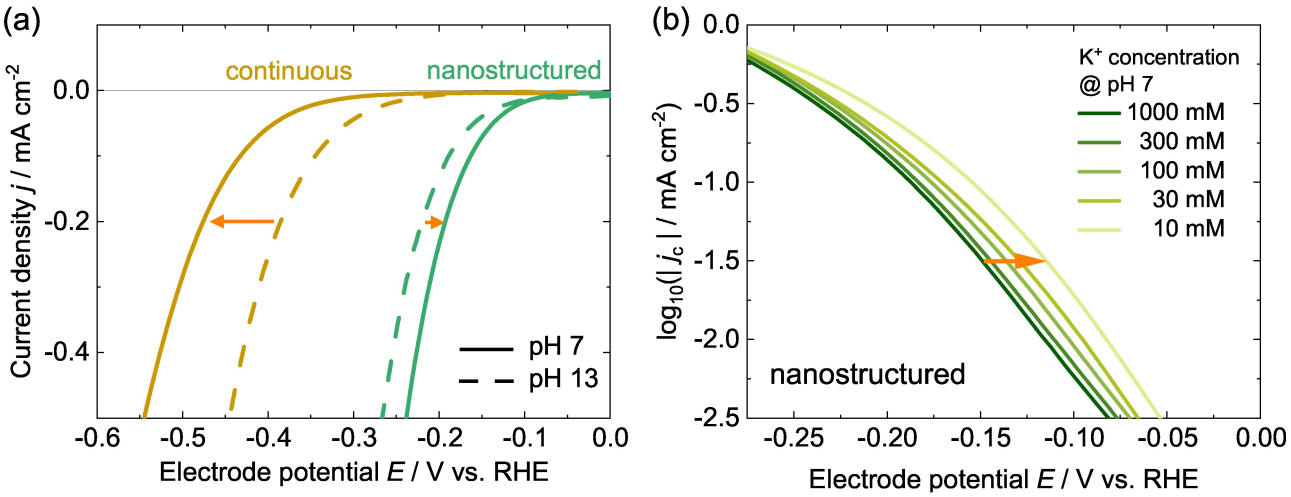

Figure 3. (a) Comparison of HER activity of the continuous Au electrode (yellow) and nanostructured Au electrode (green). The graph compares LSVs conducted in neutral medium (solid lines, 0.18 M K^+ + 0.12 M $H_2PO_4^-$/HPO_4^{2-}, pH 7) and alkaline medium (dashed lines, 0.1 M KOH, pH 13). The HER rate on nanostructured electrodes shows a reversed dependence on the pH. (b) LSVs of a nanostructured electrode in electrolytes at various (bulk) cation K^+ concentration. All electrolytes have a pH value of 7. The data is IR-corrected. The exact composition of the electrolytes is given in SI.6. The highest HER rate is obtained in the most dilute electrolyte.

Note that the electrode potential is given vs. the RHE scale. In this scale, the equilibrium potential of the HER is at the same potential, however, the point-of-zero-charge (PZC) is at a higher RHE potential for pH 13 than for pH 7, as its position is approx. the same in SHE scale.[8]

First, we consider the behavior of the continuous layer electrode (Figure 3(a) yellow lines): To attain a certain reaction current, a larger overpotential is necessary at pH 7 than at pH 13 (see orange arrow in the figure). This behavior is known from the literature for bare Au electrodes[9] and traced back to a lower net concentration of cations at the electrode surface in neutral media.[9]

Contrary, for the nanostructured electrode (Figure 3(a) green lines) both curves lie rather close to each other and even exhibit an opposite trend. To draw a given reaction current slightly less overpotential must be applied at pH 7 than at pH 13 (cf. orange arrow).

Dependence on the Bulk Cation Concentration

Last, we investigate the behavior of the HER activity of nanostructured electrodes on the (bulk) cation concentration. We analyze the activity in buffered neutral electrolytes for different (bulk) concentration of cations. Here we choose K as the cationic species present in solution. All electrolytes investigated exhibit a similar pH of 7. The exact composition of the electrolytes is given in SI.6.

Figure 3(b) shows the logarithmic scaled LSVs of the nanostructured electrode in the mentioned electrolytes. The non-faradaic current present at 0 V_{RHE} has been subtracted from the data beforehand. Clearly, the highest activity is obtained in the most diluted electrolyte, i.e. with the lowest concentration of K cations in solution, while the lowest activity is found for the strongest electrolyte.

An opposite trend is found in the literature for bare Au surfaces. Here, the highest HER activity is found for the strongest electrolyte, i.e. the electrolyte with highest concentration of cations (at moderately alkaline pH).[9] Thus the trend observed for nanostructured electrodes is, again, opposite to the behavior known from a continuous layer electrode.

Altered Reaction Mechanism of the HER at Metal/Insulator Interfaces

Based on our experimental results, we now present a HER mechanism occurring at the metal/insulator interface. This mechanism differs from the HER mechanisms known from the literature. In the subsequent section, we develop a theoretical model of the HER current at the metal/insulator interface, which supports the hypotheses made here.

At the metal/insulator interface, the HER rate is larger compared to HER rate at the metal surface. All data shown in the previous section can be interpreted consistently, when assuming that the HER enhancement at the metal/insulator interface is caused by a combination of two factors:

(I) The hydrogen adsorption process is altered due to the presence of silanol (SiOH) groups on the insulator surface.
(II) The charge transfer through the double layer is enhanced because the double layer above the insulator surface is less rigid.

Altered Hydrogen Adsorption Mechanism

In the Volmer step, water is reduced resulting in an (adsorbed) hydrogen atom and a hydroxide ion, cf. Eq. (1). At the metal/insulator interface, though, hydrogen atoms may be adsorbed by dissociating silanol groups (SiOH) present on the insulator surface according to Eq. (6):

$$SiOH + M^{*} + e^{-} \rightarrow SiO^{-} + M{-}H_{ad} \quad (6)$$

This process may occur either directly, as written, or may be mediated by one or more water molecules present above the electrode surface. This would give a Grotthuss like lateral transport of protons across the electrode surface from the insulator to the metal catalyst surface. A schematic of the process is shown in Figure 4(I).

Note that this adsorption process does not necessitate a dissociation of a water molecule above the catalyst surface. According to Koper and co-workers,[9,10] cations in the double layer reduce the activation barrier of water dissociation in the classical Volmer step. However, the dissociation of silanol groups rather than water molecules is a different mechanism and should go along with an altered cation trend.

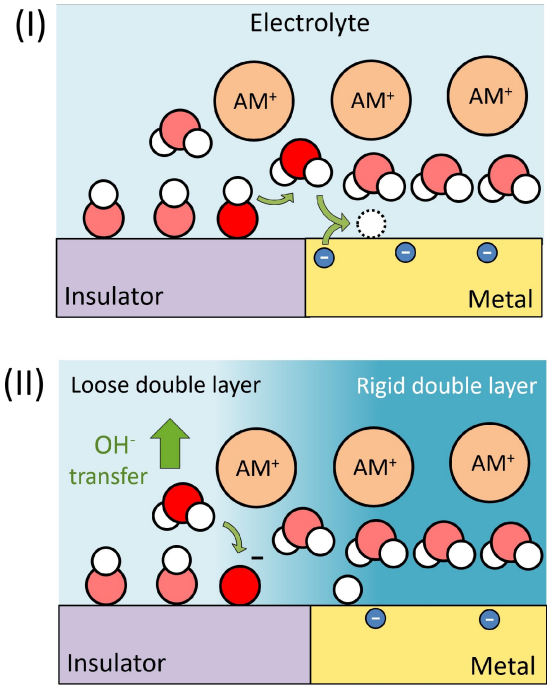

Figure 4. Scheme of the proposed mechanism enhancing the HER at metal/insulator interfaces: (I) Altered hydrogen adsorption process. The adsorbed proton stems from a dissociated silanol group on the insulator surface. (II) Water reduction and enhanced OH^{-} transport into the electrolyte at the insulator/electrolyte interface due to the lower rigidity of the double layer above the insulator surface.

Enhanced Hydroxide Ion Transfer through the Double Layer

At the metal/insulator interface, the Volmer step is then completed by the re-protonation of the silanol group (water reduction above the insulator surface), cf. Eq. (7), and the subsequent transfer of the hydroxide ion from the electrode surface through the double layer into the electrolyte bulk, cf. Eq. (8):

$$SiO^{-} + H_2O \rightarrow SiOH + OH^{-}\ (surface) \quad (7)$$

$$OH^{-}\ (surface) \rightarrow OH^{-}\ (bulk) \quad (8)$$

The transfer of hydroxide ions from the electrode surface to the electrolyte bulk thus takes place above the insulator surface, rather than above the metal surface. This process is illustrated schematically in Figure 4(II).

We suggest that the rate enhancement of HER from water reduction observed for nanostructured electrodes is due to the spatial separation of proton adsorption and water dissociation. At the metal/electrolyte interface, the entire applied voltage drops across the double layer. On the other hand, at the insulator/electrolyte interface, most of the applied voltage drops across the insulator layer. The electric potential at the insulator surface then depends mostly on the charge from SiO^{-} groups present on the surface and is in general much lower than the potential at the metal surface. Consequently, we expect that the electrolyte at the insulator/electrolyte interface is less polarized and has a lower cation concentration than the highly negatively charged Au nanoislands, i.e. the double layer is less „rigid". This lower rigidity, in turn, should facilitate the Grotthuss mechanism and, after water reduction above the insulator surface, improve the subsequent transfer of OH^{-} to the electrolyte bulk. As already mentioned before, the removal of hydroxide ions from the electrode surface can limit the HER current.[8,18] Our system provides a local tuning of this double layer rigidity and enables a fast charge/ion transfer into the electrolyte bulk, independent of the applied potential, or the choice of the actual HER catalyst (cf. SI.3).

Theoretical Model of the HER Current Based on the Electrostatic Pressure

The metal/insulator interface shows a strongly altered HER activity for various electrolyte properties compared to a continuous metal interface.

In this section, we develop a theoretical model for the HER current on heterogeneous metal/insulator interfaces based on the concept of electrostatic pressure and by using a double layer model from Huang et al.[19] and Iglic et al.[20] (see Methods). We will see that the various dependencies on experimental parameters can be consistently described theoretically on the basis of the proposed HER reaction mechanism presented in the previous section.

Silanol Coverage

According to the proposed mechanism, silanol groups (SiOH) are a reactant in the first process of the modified Volmer reaction, cf. Eq. (6). Consequently, the measured current should scale with the surface coverage f_{SiOH} of silanol groups on the insulator surface (in particular at the metal/insulator interface). In neutral to alkaline media, the surface coverage is given by $f_{SiOH} = \bar{n}_{SiOH}/(\bar{n}_{SiO^-} + \bar{n}_{SiOH})$, with $\bar{n}$ denoting the respective surface number density. The surface coverage changes with the pH, as the sites deprotonate with increasing pH according to the equilibrium reaction Eq. (9):

$$SiOH + OH^- \rightleftharpoons SiO^- + H_2O \tag{9}$$

By simulating the double layer with the above mentioned double layer model we determine f_{SiOH}. The simulation results giving the actual dependencies of f_{SiOH} on the pH, the cationic species and the bulk cation concentration are shown in SI.8. From the simulations we obtain that more strongly hydrated cations (large effective size) and smaller bulk cation concentrations yield the highest f_{SiOH}. The current we measured experimentally is indeed higher under circumstances where f_{SiOH} is also higher. Moreover, we can now explain the reversed pH trend we measured for metal/insulator interfaces, cf. Figure 3(a): At a lower pH, the concentration of SiOH is higher, resulting in a higher current density.

Spatially Varied Electrostatic Pressure at the Electrode/Electrolyte Interface

Next, we quantify the rigidity of the double layer by using the pressure P due to electrostatic forces in the double layer, which was previously considered in Refs. [21–24]. The pressure gradient at a distance x from the electrode is given by Eq. (10):[24]

$$\frac{\partial P}{\partial x} = \rho_F \mathcal{E} + \varepsilon_0(\varepsilon - 1)\mathcal{E}\frac{\partial \mathcal{E}}{\partial x} \tag{10}$$

for a relative permittivity ε that depends on the concentration of dipoles and the electric field $\mathcal{E}$. $\rho_F = \sum_i n_i z_i e$ is the free charge density due to ions in the electrolyte. Eq. (10) can be integrated to yield the pressure at the reaction plane at $x = x_{rp}$, given by Eq. (11):

$$P(x_{rp}) = P_0 - \int_{x_2}^{\infty} \frac{\partial P}{\partial x} dx \tag{11}$$

Here P_0 is the pressure in the bulk of the solution which we set to $P_0 = 1$ atm. The reaction plane is somewhere in the Stern layer, i.e. $x_{rp} < x_2$. Because the pressure is constant for $x < x_2$ (ρ_F is zero), the pressure at the reaction plane is simply $P(x_{rp}) = P(x_2)$.

We use the above mentioned double layer model to calculate $\mathcal{E}$, ρ_F and ε and consequently the pressure P above a metal (here Au) surface and above an insulator surface. The effective sizes of cations (including solvation shells) are specified using size factors γ_{AM}. Larger γ_{AM} means a larger degree of solvation. For the insulator, we assume that the applied potential ϕ_0 drops completely over the insulator layer, meaning that the double layer structure is not affected by changes in the applied potential. This is a reasonable assumption as the actual thickness of the insulator layer is much larger than the thickness of the corresponding Helmholtz layer.

Figure 5 shows the calculated pressure above the metal (yellow) and the insulator (purple) surfaces plotted against the

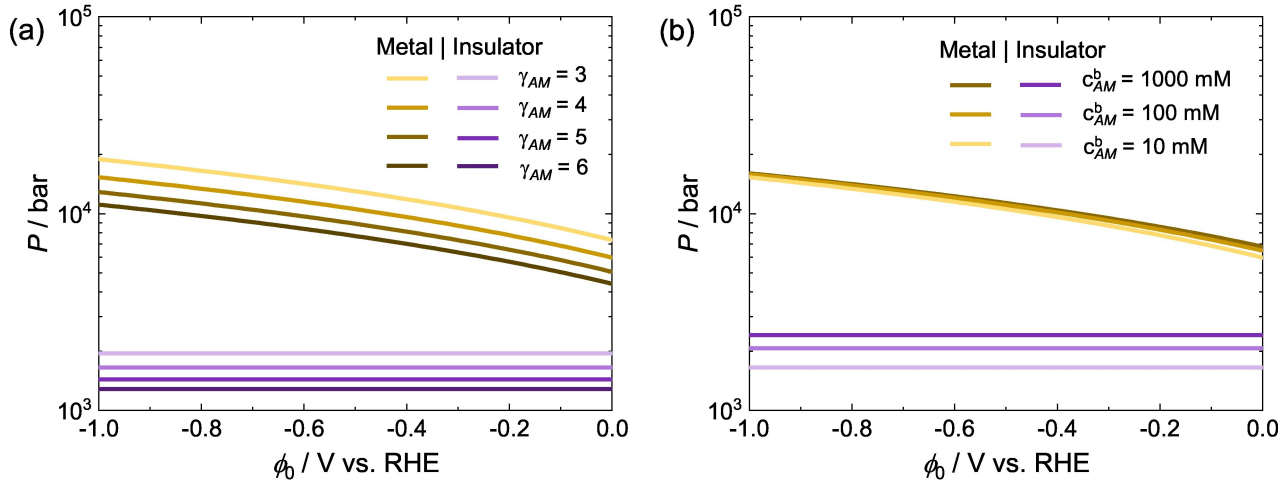

Figure 5. Simulated electrostatic pressure P in the electrolyte above the metal (Au) surface (yellow) and above the insulator surface (purple) plotted against the electrode potential ϕ_0 for (a) various effective cation sizes γ_{AM} and for (b) different cation bulk concentration c^b_{AM}. The pH is 13 in both plots. For (a), we use $c^b_{AM} = 10$ mM and for (b), we use $\gamma_{AM} = 4$. The pressure above the insulator surface is always lower than the pressure above the metal surface. In addition, the pressure above the insulator stays constant with decreasing potential, while the pressure above the metal increases.

electrode potential ϕ_0 for (a) various cation sizes γ_{AM} and (b) different bulk concentration of cations c_{AM}^{b}. By comparing the pressure at the insulator surface to the pressure at the metal surface, we can immediately see that the pressure at the insulator is an order of magnitude lower, for all cathodic potentials. The pressure force that hydroxide ions need to overcome to be transferred to the electrolyte bulk is thus indeed smaller at the insulator surface than it is at the metal surface. Consequently, water reduction and the subsequent ion transfer may be favored at the insulator surface rather than at the metal surface.

Another important observation is that the pressure increases with decreasing potential at the metal surface. On the other hand, it remains constant at the insulator surface. Consequently, the rejecting pressure force seen by OH^- ions becomes larger at the metal surface with decreasing potential, while it is independent of the potential at the insulator surface. Thus, the rate of OH^- transfer should decrease with decreasing electrode potential at a metal surface, while it is unaffected at the insulator surface. This shows the great advantage of metal/insulator interfaces compared to bare metal surfaces. The reaction rate does not become ion transfer limited, even at far negative potentials. This explains why the Tafel slope for nanostructured Au electrodes is the same as for continuous gold electrodes, cf. Figure 2(b). Despite the alteration of the proton adsorption process, the adsorption step is still rate-limiting.

Dependence of the Electrostatic Pressure on Cation Size, Bulk Concentration, and pH

A *larger* effective cation size γ_{AM} yields lower pressures above the insulator, cf. Figure 5(a). The reason is that weakly solvated cations simply pack more tightly, allowing for a larger cation concentration at the surface, which increases the pressure. A *lower* bulk cation concentration c_{AM}^{b} also gives a lower pressure, cf. Figure 5(b), as a smaller net cation concentration is expected at the surface. A *lower* pH decreases the surface charge at the insulator (see SI.8) and consequently decreases the local pressure above the insulator. On the other hand, a lower pH also shifts the equilibrium potential of the HER closer to the pzc. This, in turn, is accompanied by a lower surface charge on the metal islands and thus by a lower pressure that again enables faster ion transport through the double layer into the bulk electrolyte.

Altogether, the conditions at which we experimentally measure larger HER activities on metal/insulator interfaces (lower pH, larger solvated cations, lower cation bulk concentration) correlate with lower pressures in the double layer above the insulator.

HER Current on Nanostructured Interfaces

On the basis of the pressure, we finally elaborate a simple model for the HER current on nanostructured surfaces. We will see that the experimentally observed trends can be theoretically reproduced.

According to Marcus theory, the activation energy $\Delta G_{\ddagger}^{\ddagger}$ of an electrochemical reduction reaction depends on the overpotential η and the reorganization energy λ as given in Eq. (12):[25,26]

$$\Delta G_{\ddagger}^{\ddagger} = \frac{(\lambda + e\eta)^2}{4\lambda} \tag{12}$$

Here e is the elementary charge and η is the overpotential. The reorganization energy is typically on the order of electron volts.[25] In standard Marcus theory, λ is considered to be the reorganization of the dielectric due to the change in charge on the reactant.[25,26] From Ledezma-Yanez et al.[8] we know that the transfer of hydroxide ions from the electrode surface to the electrolyte bulk may be a crucial parameter for alkaline HER activity. Thus, in the context of HER, we replace λ by a more general „reorganization" energy Λ, which also takes into account any steric forces encountered by ions being transferred through the double layer,[1] cf. Eq. (13):

$$\Delta G_{\ddagger}^{\ddagger} = \frac{(\Lambda + e\eta)^2}{4\Lambda} \tag{13}$$

As a simple model, we now consider a linear dependence of the reorganization energy on the electrostatic pressure in the electrolyte, as given by Eq. (14):

$$\Lambda = C_1 e + C_2 (d_{H_2O})^3 P \tag{14}$$

where $(d_{H_2O})^3$ is roughly the volume of a water molecule. $C_1 e$ can be considered to be the reorganization energy in the absence of steric forces. C_2 is unitless, and can be seen as representing the number of water molecules that have to be reorganized. Here, we choose $C_1 = 6$ V such that $\Lambda > |e\eta|$ with some margin over the range of the studied parameters, and $C_2 = 3$ so that $C_2 (d_{H_2O})^3$ is roughly the volume of a solvated hydroxide ion.

Now, we use P and f_{SiOH} calculated from the double layer model, and simulate the cathodic current density j with an Arrhenius-type Ansatz, cf. Eq. (15):

$$j = -A f_{SiOH} e^{-\beta \Delta G_{\ddagger}^{\ddagger}} \tag{15}$$

Here A is a constant factor and $\beta = 1/(k_B T)$ the inverse temperature. Because electron transfer and double layer reorganization are assumed to be spatially separated, we use the potential at the metal surface to calculate the overpotential η, but we use the pressure at the insulator surface to compute Λ and consequently $\Delta G_{\ddagger}^{\ddagger}$.

[1] Note that a linear Ansatz for $\Delta G_{\ddagger}^{\ddagger}$ would later give similar trends, but we choose the form of Eq. (12) to interpret new concepts in terms of the existing theory.

Figure 6 shows the dependence of the simulated current density j as a function of the applied electrode potential ϕ_0 for (a) various cation sizes γ_{AM} and for (b) different bulk concentration of cations c^b_{AM}. The cation concentration trend observed experimentally for nanostructured electrodes, cf. Figure 3(b), is qualitatively well reproduced. For different ion sizes, the current increases in the order of scaling factors F_{AM}, cf. Eq. (5) and Figure 2(b). Note that the measured current in Figure 2(a) bottom is a superposition of the current from the inner part of the Au islands, which behave as a continuous Au surface and where HER occurs through water dissociation, and current from the metal/insulator interface regions, where HER occurs through the varied reaction process. Therefore, the differences in current with cationic species (Figure 2a) are less pronounced than in the simulation (Figure 6a).

However, these theoretical predicted dependencies agree well with the trends observed in the experimental data, and support our thesis of a modified HER mechanism at the metal/insulator interface.

Conclusions

In conclusion, we presented here a novel mechanism for the Hydrogen Evolution Reaction from water reduction at a metal/insulator interface. The mechanism comprises two processes: (I) A modified hydrogen adsorption mechanism, in which silanol groups on the insulator surface act as the proton donors. (II) The water reduction and subsequent hydroxide ion transfer occurs above the insulator surface, where the electrostatic pressure is much smaller than above the metal surface. These processes correspond to the reaction Eqs. (16) and (17), respectively:

$$SiOH + M^* + e^- \rightarrow SiO^- + M{-}H_{ad} \quad (16)$$

$$SiO^- + H_2O \rightarrow SiOH + OH^- \ (bulk) \quad (17)$$

The mechanism was deduced from the strongly altered behavior of nanostructured electrodes compared to continuous metal layers when changing several electrolyte properties, such as the cationic species, the cation concentration or the pH value of the electrolyte. With a theoretical model of the HER current based on the electrostatic pressure the experimentally observed trends were reproduced. The use of metal/insulator interfaces tunes the electrode properties in such an advantageous way that the alkaline HER rate can be enhanced by a factor of 40 on the given nanostructured surface.

While we demonstrated the strongly enhanced activity for the alkaline HER on Au/silicon nitride nanostructured surfaces, the principles governing reaction rates at metal/insulator interfaces do not depend on the system under consideration and thus should be applicable to other electrocatalytic reactions as well. The composite interfaces allow for a lateral tailoring of the double layer properties and, thus, reaction conditions. The usage of insulators as a proton source for hydrogenation reactions is an easy method to solve drawbacks stemming from fundamental properties of electrochemical interfaces in alkaline media. Equally important is the possibility to adjust the electrostatic pressure, i.e. the rigidity of the double layer, above the insulator surface by varying the insulator surface charge. This can be done independently of the applied voltage and, thus, independently of the pressure above the catalyst. Hence, the mechanism discussed here should be transferable to other reactions such as the oxygen evolution reaction and the oxygen reduction reaction. In conclusion, knowledge of these fundamental processes opens up novel design possibilities for efficient electrocatalysts in the future.

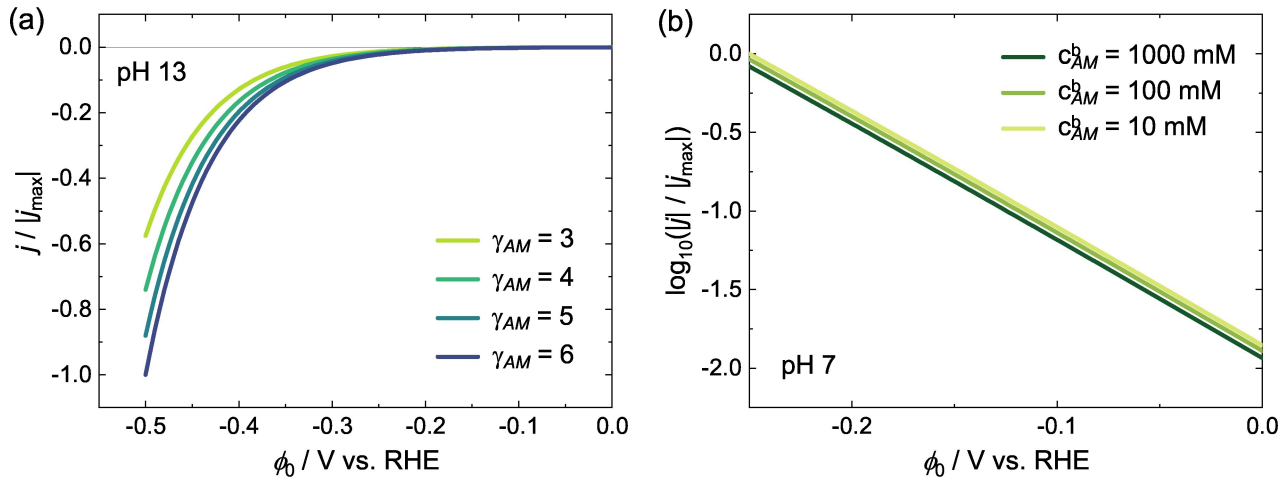

Figure 6. Simulated current density j plotted against electrode potential ϕ_0 for (a) various cation sizes γ_{AM} and (b) different bulk cation concentrations c^b_{AM}. The current density is normalized to the largest absolute value in the plotted potential range, $|j_{max}|$. Conditions are the same as for the experimental data: For (a), the pH is 13 and c^b_{AM} = 0.1 M, cf. Figure 2(a). For (b), the pH is 7 and we choose γ_{AM} = 4, cf. Figure 3(b). The experimental trends are well reproduced.

Experimental Methods

Electrode Fabrication

The metal arrays on the electrodes investigated in this work are produced by Lift-off Nanoimprint Lithography.[3,27,28] More information about the fabrication procedure is given in the references. The surface area covered by the nanostructure array expands over 5×5 cm^2. The silicon substrates used for nanostructuring are prepared from a commercial silicon wafer (n-doped, FZ: (111), 1–10 Ω cm, Si-Mat Silicon Materials, Germany), which came already covered by a LPCVD silicon nitride (Si_3N_4) layer with a thickness of 17 nm. This layer is isotropically etched in an reactive ion etching process to the desired thickness of 12 nm.

Electrochemical Measurements

The electrochemical cell used for the experiments is a custom-built, air tight three-compartment cell made of PCTFE. Its front is covered by a glass cover window made from hardened mineral glass. The three compartments (resp. containing working, reference and counter electrode) are separated from each other by a proton conducting membrane (Nafion™, Chemours, USA) to avoid cross-contamination between the compartments. The reference electrode used is a commercial Mercury/Mercurous Sulfate (MSE) reference electrode (International Chemistry Co. Ltd., Japan) which contains saturated K_2SO_4 solution. The measured electrode potential in MSE scale is converted in SHE scale using an offset of 0.64 volt.[29] We use a coiled gold-wire as the counter electrode.

All electrolytes used here are mixed from suprapur grade salts and 18.2 MΩ cm DI-Water (Elga Purelab, Veolia Water Technologies, Germany). The electrolytes are saturated with Ar gas (purity 5.0, Westfahlen, Germany) prior the electrochemical experiments.

Linear sweep voltammetric scans and cyclic voltammetric scans are conducted with a scan rate of 50 mV s^{-1}. The Tafel analysis is performed by analyzing the logarithmic plotted data of the scans. The fits were obtained in a potential window between −0.25 V_{RHE} and −0.4 V_{RHE}. Tafel slopes and exchange current densities given here are averages over three individual measurements (i.e. electrodes).

Surface Determination

All measured currents are normalized to the active surface area of the respective electrode. The electrochemical active surface area of the Au-based electrodes was determined via the OH desorption current in 0.1 M H_2SO_4 (suprapur grade, Merck) in cyclic voltammetric experiments. As an upper potential limit 1.75 V_{RHE} was chosen, as it has been found to be the approximate potential at which a „monolayer-like coverage" is achieved.[30] The transferred charge during the subsequent gold oxide reduction process was divided by 390 μC cm^{-2}, which is the well accepted specific surface charge value for Au surfaces.[29,31] In the SI.7, exemplary CVs of a continuous Au-layer electrode in 0.1 M H_2SO_4 in the Au oxidation region and the determined charge transferred during the AuOx reduction process as a function of the upper turning potential is shown.

The surface area of the individual electrodes was determined before and after the HER experiments. It turned out that the change during the experimental procedure never exceeded 5 %.

Computational Methods

Double Layer Model

We model the local reaction conditions in the electric double layer by using the double layer model from Huang et al.[19] and Iglic et al.[20] In this model, the electric potential ϕ is described by a modified Poisson-Boltzmann equation given by Eq. (18):

$$-\frac{\partial}{\partial x}\left[\varepsilon_0\varepsilon(x)\frac{\partial\phi}{\partial x}\right]=\sum_i z_i e n_i(x) \tag{18}$$

Here ε_0 is the vacuum permittivity, ε the relative permittivity, e the elementary charge, and z_i and n_i are the charge number and number density of species i in the electrolyte, respectively. We include protons, hydroxide ions, alkali metal cations AM, anions X, and water molecules: $i \in \{H^+, OH^-, AM, X, H_2O\}$. An overview of the parameters in the model can be found in SI.10.

The relative permittivity ε depends on the local electric field $\mathcal{E}=-\partial\phi/\partial x$ and number density of (polarizable) water molecules n_{H_2O} via Eq. (19):

$$\varepsilon(x)=\varepsilon_\infty+\frac{p n_{H_2O}(x)}{\mathcal{E}(x)}\mathcal{L}(\beta p\mathcal{E}(x)) \tag{19}$$

with ε_∞ the optical permittivity, p the dipole moment, and $\mathcal{L}(y)=\coth(y)-1/y$ the Langevin function. To find p consistent with the bulk permittivity of water $\varepsilon_w \approx 78.5$, we note that $\mathcal{E}=0$ in the bulk. From Eq. (19) it then follows that $\varepsilon_w=\varepsilon_\infty+\frac{1}{3}\beta p^2 n_w$, or that p is given by Eq. (20):

$$p=\sqrt{\frac{3(\varepsilon_w-\varepsilon_\infty)}{\beta n_w}} \tag{20}$$

with the bulk number density of pure water $n_w=55.5\ \mathrm{M}\times N_A$.

The finite size of ions in the electrolyte is accounted for by considering a lattice with lattice spacing d_{H_2O}, the effective diameter of a water molecule. This effective diameter is calculated such that $n_w=(d_{H_2O})^{-3}$ which yields $d_{H_2O}\approx 3.1$ Å. Ions may occupy multiple lattice sites; their effective (i.e. including solvation shell) sizes are specified using the relative size factor given by Eq. (21):

$$\gamma_i=\left(\frac{d_i}{d_{H_2O}}\right)^3 \tag{21}$$

with d_i the effective diameter of species i. Ions with a high degree of solvation such as Li^+ have a large effective size; weakly solvated ions like Cs^+ have a small effective size. Drab et al.[32] inferred from bulk permittivity data that $\gamma_{AM}+\gamma_X\approx 7.5$ for NaCl electrolytes. Because the solvation shells of ions are not fixed, it is difficult to connect values of γ to the actual size of ions. Here, we investigate cation size trends qualitatively by considering γ_{AM} =3, 4, 5, 6, which are considered to be in the range of the cations used experimentally.

Using these size factors, the number densities n_i are written as a fraction of the lattice site density $n_{max}=(d_{H_2O})^{-3}$ (= n_w) via Eq. (22):

$$n_i=n_{max}\frac{\chi_i\Theta_i(x)}{\sum_j\gamma_j\chi_j\Theta_j(x)} \tag{22}$$

where n_i^b is the bulk number density of species i and $\chi_i = n_i^b/n_{max}$. Θ_i are Boltzmann factors, defined as given in Eq. (23):

$$\Theta_i(x) = \begin{cases} \exp(-\beta z_i e\phi(x)), & \text{for } i \in \{H^+, OH^-, AM, X\} \\ \frac{\sinh \beta p\mathcal{E}(x)}{\beta p\mathcal{E}(x)}, & \text{for } i = H_2O \end{cases} \quad (23)$$

Note that if $\Theta_i \gg \Theta_j$ for all j, n_i approaches a saturation limit concentration of n_{max}/γ_i.

As potential reference, we choose the point of zero charge (PZC) of gold, which was measured to be $E_{PZC,Au} = 0.2\ V_{SHE}$ for the electrodes considered in this work.[33] A potential with respect to this PZC can be converted to a potential with respect to RHE as given in Eq. (24):

$$\phi(\text{vs. RHE}) = \phi(\text{vs. PZC}) + E_{PZC,Au} + 59\ \text{mV} \times \text{pH} \quad (24)$$

The boundary conditions to Eq. (18) are specified as follows. First, in the solution bulk, $\phi = 0$ V vs. PZC. At the electrode, the boundary conditions are specified on the plane of closest approach for ions at distance x_2 from the electrode surface. Here, we consider $x_2 = d_{AM}/2$, as we only consider potentials negative of the point of zero charge of gold and so the plane of closest approach is set by the size of the cations. The potential at x_2 is denoted $\phi_2 = \phi(x_2)$.

Metal Boundary Condition

Between the electrode surface and x_2, there are no free charges, so the potential profile is linear. For metal surfaces at potential ϕ_0, the boundary condition is then given by Eq. (25):

$$-\mathcal{E}(x_2)x_2 = \phi_2 - \phi_0 \quad (25)$$

Insulator Boundary Condition

Van Hal et al.[34] derived the surface charge at insulator surfaces with acidic surface OH groups as given by Eq. (26):

$$\sigma = -e\bar{n}_{sil}\frac{K_a}{K_a + c_{H^+}^b \exp(-\beta e\phi_0)} \quad (26)$$

Here $c_{H^+}^b$ is the bulk concentration of protons (although it is small in alkaline medium, it gives the same result as when rewriting the fraction in terms of $c_{OH^-}^b$). $\bar{n}_{sil} = 5\times10^{18}\ m^{-2}$ is the areal density of silanol (SiOH and SiO^-) sites and $K_a = 10^{-6}$ M is the acid dissociation constant for silanol – these values are used for silica by van Hal et al.;[34] silicon nitride should behave similarly. Together with Eq. (25) and $\sigma = \varepsilon_0\varepsilon(0)\mathcal{E}(0) = \varepsilon_0\varepsilon(x_2)\mathcal{E}(x_2)$, the boundary condition for silica surfaces is finally given by Eq. (27):

$$\varepsilon_0\varepsilon(x_2)\mathcal{E}(x_2) = -e\bar{n}_{sil}\frac{K_a}{K_a + c_{H^+}^b \exp(-\beta e(\phi_2 + \mathcal{E}(x_2)x_2))} \quad (27)$$

The fraction f_{SiOH} of protonated silanol sites is calculated as:

$$f_{SiOH} = \left(1 - \frac{-\sigma/e}{\bar{n}_{sil}}\right)$$

Details on the numerical implementation of the model can be found in SI.9.

Acknowledgements

The authors thank Dr. Jun Huang for his help with the numerical implementation of the double layer model. The authors gratefully acknowledge the support by Deutsche Forschungsgemeinschaft (DFG, German Research Foundation) through "e-conversion Cluster of Excellence", EXC 2089/1-390776260, and through TUM International Graduate School of Science and Engineering (IGSSE), GSC 81-24184165, and the support by the Bavarian State Ministry of Science and the Arts within the Collaborative Research Network "Solar Technologies go Hybrid (SolTech)". Open Access funding enabled and organized by Projekt DEAL.

Conflict of Interests

There is no conflict of interest.

Data Availability Statement

The data that support the findings of this study are available from the corresponding author upon reasonable request.

Keywords: HER · gold · silicon · nanostructures · cations

[1] R. Subbaraman, D. Tripkovic, D. Strmcnik, K.-C. Chang, M. Uchimura, A. P. Paulikas, V. Stamenkovic, N. M. Markovic, *Science* **2011**, *334*, 1256.
[2] N. Danilovic, R. Subbaraman, D. Strmcnik, K.-C. Chang, A. P. Paulikas, V. R. Stamenkovic, N. M. Markovic, *Angew. Chem.* **2012**, *124*, 12663.
[3] T. L. Maier, M. Golibrzuch, S. Mendisch, W. Schindler, M. Becherer, K. Krischer, *J. Chem. Phys.* **2020**, *152*, 154705.
[4] X. Wu, W. Li, S. Sheng, L. Zhu, L. Yuan, J. Liu, S. Jin, Z. Zhang, *Electrochem. Commun.* **2021**, *129*, 107085.
[5] X. Chen, I. T. McCrum, K. A. Schwarz, M. J. Janik, M. T. M. Koper, *Angew. Chem. Int. Ed.* **2017**, *56*, 15025.
[6] S. Xue, B. Garlyyev, S. Watzele, Y. Liang, J. Fichtner, M. D. Pohl, A. S. Bandarenka, *ChemElectroChem* **2018**, *5*, 2326.
[7] N. Danilovic, R. Subbaraman, D. Strmcnik, A. P. Paulikas, D. Myers, V. R. Stamenkovic, N. M. Markovic, *Electrocatalysis* **2012**, *3*, 221.
[8] I. Ledezma-Yanez, W. D. Z. Wallace, P. Sebastian-Pascual, V. Climent, J. M. Feliu, M. T. M. Koper, *Nat. Energy* **2017**, *2*.
[9] A. Goyal, M. T. M. Koper, *Angew. Chem. Int. Ed.* **2021**, *60*, 13452.
[10] M. C. O. Monteiro, A. Goyal, P. Moerland, M. T. M. Koper, *ACS Catal.* **2021**, *11*, 14328.
[11] D. V. Esposito, I. Levin, T. P. Moffat, A. A. Talin, *Nat. Mater.* **2013**, *12*, 562.
[12] D. Strmcnik, P. P. Lopes, B. Genorio, V. R. Stamenkovic, N. M. Markovic, *Nano Energy* **2016**, *29*, 29.
[13] S. Filser, T. L. Maier, R. D. Nagel, W. Schindler, P. Lugli, M. Becherer, K. Krischer, *Electrochim. Acta* **2018**, *268*, 546.
[14] I. T. McCrum, M. T. M. Koper, *Nat. Energy* **2020**, *5*, 891.
[15] F. J. Sarabia, P. Sebastian-Pascual, M. T. Koper, V. Climent, J. M. Feliu, *ACS Appl. Mater. Interfaces* **2018**, *11*, 613.
[16] L. Rebollar, S. Intikhab, J. D. Snyder, M. H. Tang, *J. Electrochem. Soc.* **2018**, *165*, J3209.
[17] S. Mezzasalma, D. Baldovino, *J. Colloid Interface Sci.* **1996**, *180*, 413.
[18] J. T. Bender, A. S. Petersen, F. C. Ostergaard, M. A. Wood, S. M. Heffernan, D. J. Milliron, J. Rossmeisl, J. Resasco, *ACS Energy Lett.* **2022**, *8*, 657.
[19] J. Huang, M. Li, M. J. Eslamibidgoli, M. Eikerling, A. Groß, *JACS Au* **2021**, *1*, 1752.
[20] A. Iglič, E. Gongadze, V. Kralj-Iglič, *Acta Chim. Slov.* **2019**, *66*, 534.
[21] W. Dreyer, C. Guhlke, R. Müller, *Phys. Chem. Chem. Phys.* **2013**, *15*, 7075.
[22] W. Dreyer, C. Guhlke, M. Landstorfer, *Electrochem. Commun.* **2014**, *43*, 75.

[23] M. Landstorfer, C. Guhlke, W. Dreyer, *Electrochim. Acta* **2016**, *201*, 187.
[24] M. Landstorfer, R. Müller, *Electrochim. Acta* **2022**, *428*, 140368.
[25] W. Schmickler, E. Santos, *Interfacial Electrochemistry*, Springer, Berlin, Heidelberg **2010**.
[26] J. Huang, *J. Chem. Phys.* **2020**, *153*.
[27] R. D. Nagel, S. Filser, T. Zhang, A. Manzi, K. Schönleber, J. Lindsly, J. Zimmermann, T. L. Maier, G. Scarpa, K. Krischer, P. Lugli, *J. Appl. Phys.* **2017**, *121*, 084305.
[28] M. Golibrzuch, T. L. Maier, M. J. Feil, K. Krischer, M. Becherer, *J. Appl. Phys.* **2022**, *131*, 124301.
[29] A. J. Bard, L. R. Faulkner, *Electrochemical Methods: Fundamentals and Applications*, Wiley **2001**.
[30] A. Hamelin, *J. Electroanal. Chem.* **1996**, *401*, 1.
[31] S. Trasatti, O. A. Petrii, *Pure Appl. Chem.* **1991**, *63*, 711.
[32] M. Drab, E. Gongadze, L. Mesarec, S. Kralj, V. Kraljlglic, A. lglic, *Elektrot. Vestnik* **2017**, *84*, 221.
[33] T. L. Maier, *Enhancing the Hydrogen Evolution Reaction on Nanostructured Metal/Silicon Electrodes by a Bifunctional Mechanism*, Ph.D. thesis, Technische Universität München **2023**.
[34] R. van Hal, J. C. Eijkel, P. Bergveld, *Adv. Colloid Interface Sci.* **1996**, *69*, 31.

Manuscript received: February 2, 2024
Revised manuscript received: March 18, 2024
Version of record online: May 16, 2024